# Electronic and transport properties of azobenzene monolayer junctions as molecular switches

Yan Wang(王琰) and Hai-Ping Cheng
*Department of Physics and Quantum Theory Project, University of Florida, Gainesville, Florida 32611, USA*
(Received 22 March 2012; published 26 July 2012)

We investigate from first principles the change in transport properties of a two-dimensional azobenzene monolayer sandwiched between two Au electrodes that undergoes molecular switching. We focus on transport differences between a chemisorbed and physisorbed top monolayer-electrode contact. The conductance of the monolayer junction with a chemisorbed top contact is higher in the *trans* configuration, in agreement with the previous theoretical predictions of one-dimensional single-molecule junctions. However, with a physisorbed top contact, the ON state, with larger conductance, is associated with the *cis* configuration due to a reduced effective tunneling pathway, which successfully explains recent experimental measurements on azobenzene monolayer junctions. A simple model is developed to explain electron transmission across subsystems in the molecular junction. We also discuss the effects of monolayer packing density, molecule tilt angle, and contact geometry on the calculated transmission functions. In particular, we find that a tip-like contact with chemisorption significantly affects the electric current through the *cis* monolayer, leading to highly asymmetric current-voltage characteristics as well as large negative differential resistance behavior.

DOI: 10.1103/PhysRevB.86.035444 PACS number(s): 85.65.+h, 31.15.E−, 73.50.−h

## I. INTRODUCTION

Molecular junctions that incorporate photochromic molecules as reversible photoswitches between two different conductance states (ON and OFF) have advanced considerably in the last decade.[1,2] Azobenzene and its derivatives are the most frequently studied candidates for a photoresponsive molecular switch, based on their conformational changes from a more thermodynamically stable *trans* configuration to a *cis* configuration in response to an external stimulus such as UV light,[3] and vice versa upon exposure to visible light or thermal excitation.[4] Previous first-principles studies for azobenzene molecular junctions focused on electron transport through ideal single-molecule junctions with one-dimensional (1D) electrodes and predict that the junction with the *trans* configuration has a conductance higher than that with the *cis* configuration.[5–7]

More recent attention in experiments has been paid to the self-assembled monolayer (SAM) systems, which are highly ordered arrays of molecules on a two-dimensional (2D) surface with a chemisorbed bottom contact. A variety of experimental methods have been used to apply a second contact on top of the azobenzene SAM and measure the photoinduced changes in its conductance, with sufficient flexibility to adapt to the height change of the SAM after its photoswitch, including liquid metal contact (e.g., Hg drop[8]) and conducting atomic force microscopy.[9,10] These pioneering experiments found that the ON state with a larger measured current is associated with the *cis* configuration, contrasting previous theoretical predictions based on single-molecule junction models.

These experiments using 2D monolayer junctions present more complicated situations in which the ideal 1D single-molecule junction model may not apply. First, in the monolayer junction the two monolayer-electrode contacts are not symmetric. The one at the bottom interface is a chemisorbed contact, in which the end group of the molecule is chemically bonded to the electrode. The top contact is merely physical, i.e., no chemical bonding is formed between the SAM and the top electrode. It is known that the way the molecule interacts with the electrode plays a crucial role in electronic transport through the molecule. The conductance of a junction with and without chemicontacts can differ by several orders of magnitude.[11,12] In addition, SAMs can form with differences in packing density and tilt angle, and in densely packed SAMs the conductance may involve both intramolecular and intermolecular contributions due to molecules in close proximity.[13] Other effects such as the surface topography and roughness of the contact also influence the final geometry of the contact and thus lead to more complex transport properties. These uncertainties in the microscopic details of a monolayer junction make understanding the effects of monolayer-electrode coupling, intermolecular interaction, and contact geometries critical to elucidating its transport mechanisms. First-principles studies are especially valuable in this regard because information concerning the microscopic details of a monolayer junction and their effects on electron transport are often impossible to obtain directly in experiments.

Here we report a first-principles study of the electronic structure and transport properties of azobenzene monolayer junctions. The monolayer junction is constructed by attaching a Au(111) electrode on top of an azobenzene monolayer chemisorbed on a Au(111) substrate. We focus on clarifying the role of monolayer-electrode bonding in relation to the transport properties by investigating the junctions with two types of top monolayer-electrode contact: (1) a strongly bonded contact in which the molecules are covalently bonded to the Au surface, and (2) a weakly bonded contact which is physisorbed through the van der Waals (vdW) interaction. We find that both the *trans* to *cis* transformation of the molecules and the monolayer-electrode bonding play critical roles in determining the electron transmission as well as the current-voltage characteristics of the monolayer junction. The impact of monolayer packing density and tilt angle are discussed. We also consider the effect of contact geometry by adding an additional Au atom at the top contact and find substantive changes in transport depending on this particular contact geometry.

 

## II. COMPUTATIONAL METHODS

We use two density-functional theory (DFT) based computational methods in our calculations. First, all structural optimizations, including calculations for both the azobenzene monolayer on a Au(111) surface and the molecular junction consisting of two monolayer-electrode contacts, are performed using the plane-wave-basis-set Vienna *ab initio* simulation package (VASP).[14] Then, electron transport calculations of the molecular junction are performed using the atomic-orbital-basis-set TRANSIESTA code,[15] which incorporates a nonequilibrium Green's function formalism[16] and DFT treatment of the electronic structure as implemented in the SIESTA package.[17]

In the structural optimization calculations, projector augmented wave potentials with kinetic energy cutoff of 400 eV are employed. For the exchange and correlation functional we utilize the Perdew-Burke-Ernzerh generalized gradient approximation (PBE-GGA).[18] A $3 \times 3 \times 1$ $k$-point sampling is applied based on the Monkhorst-Pack[19] scheme. All geometries are optimized until the remaining force on each ion falls below the convergence criterion of 0.02 eV/Å.

In the electron transport calculations, we utilize norm-conserving nonlocal Troullier-Martins pseudopotentials and the PBE-GGA exchange correlation functional, with a single-$\zeta$ plus polarization basis for the Au atoms and a higher level double-$\zeta$ basis set for the molecules. The equivalent plane-wave cutoff for the real-space grid of 150 Ry is used throughout the calculations. A $5 \times 5 \times 1$ Monkhorst-Pack $k$-point sampling is used for self-consistent calculation, and a $9 \times 9k$-point sampling is used for transmission calculations. The transmission function is obtained by averaging transmission coefficients in each $k$ point for an applied bias voltage $V$, $T(E,V) = \sum_{k_x,k_y} T_{k_x,k_y}(E,V)$, where

$$T_{k_x,k_y} = \mathrm{Tr}[\Gamma_1 G^R \Gamma_2 G^A] \quad (1)$$

is the $k$-resolved transmission coefficient, $G^{R,A}$ are the retarded (advanced) Green's function matrices, and $\Gamma_{1,2} = i[\Sigma_{1,2} - \Sigma_{1,2}^\dagger]$ where the $\Sigma_{1,2}$ are the retarded self-energies due to the existence of bottom (top) semi-infinite electrodes. The electric current as a function of the applied voltage is obtained by the integration of the transmission function

$$I(V) = \frac{2e}{h} \int T(E,V)[f(E-\mu_1) - f(E-\mu_2)]dE, \quad (2)$$

where $e$ is the elementary charge, $f$ is the Fermi-Dirac distribution function, and $\mu_{1,2} = E_F \pm eV/2$ are the chemical potentials for the bottom (top) electrodes.

## III. AZOBENZENE MOLECULAR MONOLAYER ON Au(111) SURFACE

### A. Structural models

For the azobenzene monolayer on the Au(111) substrate (hereafter we denote this as Au-AB), the systems that we study consist of an azobenzene monolayer chemisorbed on the surface of the Au(111) substrate by a $CH_2S$ linker for each molecule, as illustrated in Fig. 1 produced by VESTA graphical program.[20] The substrate is modeled by a slab consisting of five Au(111) layers. The molecular coverage is kept fixed at one molecule per $(\sqrt{3} \times \sqrt{3})R30^\circ$ surface unit cell, which corresponds to a packing area of 90.8 Å per molecule. The supercell thus consists of 87 atoms comprising 12 atoms per Au layer and 27 atoms for the azobenzene molecule with the linker. A large vacuum spacing of 15 Å is used between the topmost molecular atom and the next Au slab to prevent interaction between adjacent images. All atoms except the two bottom Au layers are fully relaxed.

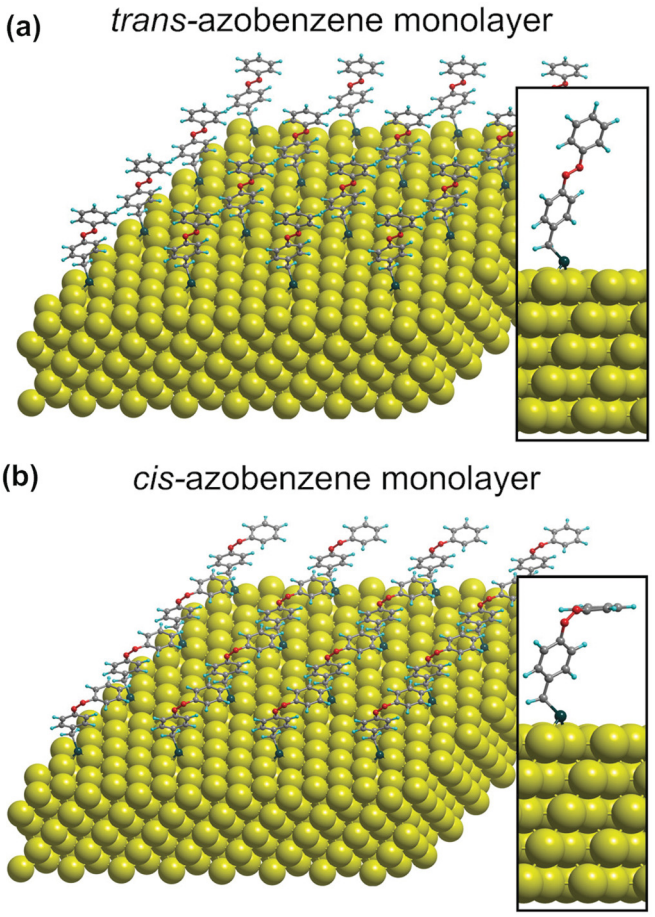


FIG. 1. (Color online) Equilibrium configurations of *trans* and *cis*azobenzene molecules chemisorbed on the Au(111) surface via a $CH_2S$ linker. Insets: side view of the corresponding geometry. C, H, N, S, and Au atoms are colored gray, green, red, blue, and yellow, respectively.

### B. Adsorption geometry and energetics

To determine the preferred adsorption position for the azobenzene monolayer on the Au(111) surface, three possible initial binding sites of both azobenzene isomers with the bottom $CH_2S$ linker are optimized on the Au(111) surface, the on-top site and the fcc- and hcp-bridge sites, as shown in Fig. 2. The calculated total energy and binding energy of an azobenzene molecule at different adsorption sites are reported in Table I. For both *trans* and *cis* configurations, we find the most stable adsorption position to be the fcc-bridge site. We also find the *trans* configuration to be more stable by about 0.6 eV than the *cis* configuration, in good agreement with the results from previous calculations[21] and experiment.[22] Bader analysis based on the real-space charge density[23] for

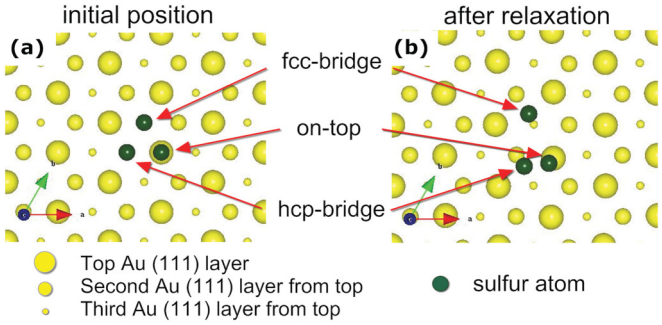


FIG. 2. (Color online) Top view indicating the lateral position of the sulfur atom in the structural optimizations carried out to determine the most stable adsorption site of the azobenzene molecule with $CH_2S$ linker on Au(111) surface: (a) initial position; (b) the optimized position.

the Au-AB shows a small amount of charge transfer from Au substrate to the molecule for all cases, as given in Table I. The charge transferred to the molecule is primary localized at the $CH_2S$ linker, and not efficiently shared with the core part of the molecule. Hereafter we present only the results for systems with the azobenzene monolayer chemisorbed on the fcc-bridge site of the Au(111) surface.

We also optimize the tilt angle of the azobenzene monolayer on the Au(111) surface. In Fig. 3 we show the calculated total energy of a *trans* azobenzene monolayer on Au(111) as a function of tilt angle ranging from 10° to 45°. At every single energy point in Fig. 3, the monolayer structure is optimized by performing geometry relaxation with an initially given tilt angle. Within this angle range, we find that the lowest energy structure is the 20° tilted molecule chemisorbed on the Au(111) surface. We expect the same finding for the *cis* configuration since the *trans* to *cis* transformation only changes the geometry of the top half of the azobenzene molecule. Therefore, for the rest of the study we choose the azobenzene monolayer with a tilt angle of 20° as the equilibrium structure for both *trans* and *cis* configurations, as shown in Fig. 1.

However, it should be noted that in Fig. 3 the calculated total energies of these systems with different tilt angles are very close. In experiments, the tilt angle of molecules in the monolayer is usually determined by other factors, such as ambient temperature and monolayer packing density. It has been found that the molecular monolayer undergoes a phase transition from a tilted structure to a vertical structure at room

TABLE I. Calculated total energy (in eV per molecule), binding energy (in eV per molecule) and charge transfer (in $|e|$) of an azobenzene molecule on Au(111) surface at different adsorption sites. The total energy of Au/*trans* AB at fcc-bridge site is set to be reference zero.

| Isomer type | Adsorption site | $E_{\text{total}}$ | $E_b$ | Charge transfer |
|---|---|---|---|---|
| *trans* | fcc-bridge | 0 | 2.084 | 0.07 |
| | hcp-bridge | 0.110 | 1.974 | 0.07 |
| | on-top | 0.398 | 1.686 | 0.08 |
| *cis* | fcc-bridge | 0.635 | 2.112 | 0.08 |
| | hcp-bridge | 0.700 | 2.037 | 0.07 |
| | on-top | 1.052 | 1.695 | 0.06 |

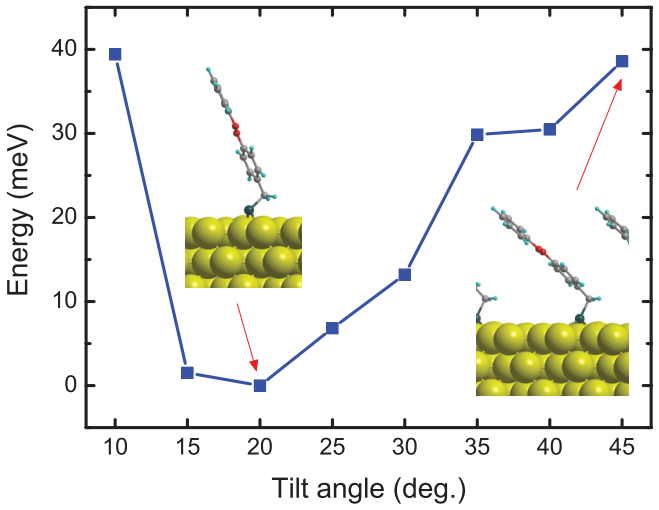


FIG. 3. (Color online) Total energy as a function of tilt angle for *trans* azobenzene molecules chemisorbed on Au(111) surface. The left and right insets are side views of the corresponding optimized structures with tilt angles of 20° and 45°, respectively.

temperature.[24] Also, in densely packed monolayers at full coverage, monolayers with a small tilt angle can be generally expected, with molecules standing with their long molecular axes close to the surface normal.

### C. Electronic structure

Figure 4 analyzes the interaction between the azobenzene and Au(111) surface in terms of the density of states projected onto the atoms (PDOS) in the molecule as well as the sulfur linker. For both *trans* and *cis* configurations, we see that the two frontier orbital levels of azobenzene—the highest

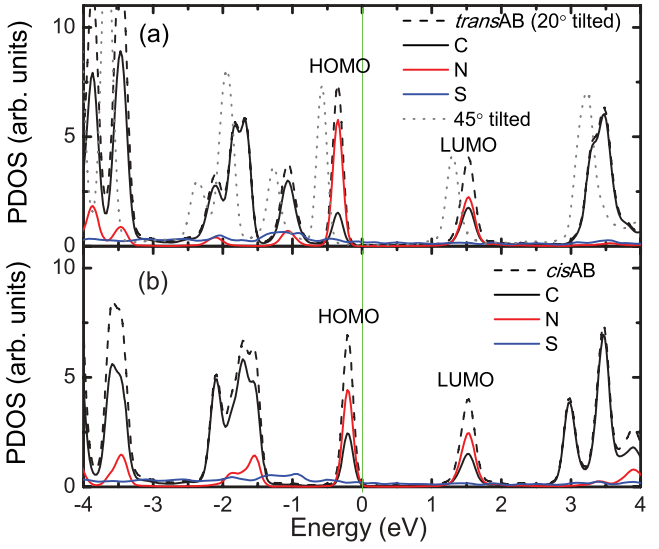


FIG. 4. (Color online) Projected density of states of the molecule and various atoms of *trans* (a) and *cis* (b) azobenzene monolayer chemisorbed on Au(111) surface. For the*trans* configuration, additionally shown is the PDOS of the molecule with a tilt angle of 45° on the Au surface. The vertical green line represents the Fermi energy, which is at 0 eV.

occupied molecular orbital (HOMO) and the lowest unoccupied molecular orbital (LUMO)—lie at each side of the Au Fermi level. Unlike the other molecular orbital levels nearby, the HOMO and LUMO contain large contributions from the nitrogen pair of the azobenzene. The position of HOMO in the *cis* configuration is closer to the Au Fermi level than that in the *trans* configuration. This is quite different from the results of a study of a single azobenzene molecule on an Au(111) surface,[21] in which the downshift of molecular orbital level is more significant for the *cis* isomer, resulting in the HOMO of *cis* azobenzene being away from the Au Fermi energy and its LUMO being very close to the Fermi energy. This difference arises because the azobenzene molecules in the monolayer are standing upright (nearly perpendicular to the surface), resulting in a weak interaction between the molecule and the bottom surface, whereas a single azobenzene molecule orients parallel to the surface and thus the closer proximity between the azo group (N pair) of the molecule and the Au surface creates a stronger interaction between them.[21,25] For the *trans* monolayer with a tilt angle of 45° on the Au surface, we find essentially the same features in the PDOS as obtained for the 20° tilted *trans* monolayer, but all molecular orbital levels are roughly equally shifted by about 0.4 eV to lower energies.

## IV. AZOBENZENE MONOLAYER JUNCTIONS AND TRANSPORT PROPERTIES

### A. Structural models and electronic structures

Once the equilibrium geometry of the Au-AB is obtained, we construct the corresponding molecular junction by extending the bottom Au(111) substrate into a six atomic layer slab, and attaching a second Au(111) slab consisting of another six atomic Au layers on top of the azobenzene monolayer. To examine the effect of monolayer-electrode contact, two types of interfacial contacts for the top electrode are studied: (1) the top Au surface is covalently bonded to the azobenzene monolayer with $CH_2S$ linkers same as those at the bottom contact (hereafter we denote this type of junction as Au-AB-Au), and (2) the top contact is physisorbed on the azobenzene monolayer surface without the $CH_2S$ linkers (we denote this as the Au-AB|Au junction). We optimize the top interfacial contact by computing the total energies of the system as a function of the distance between the left and right electrodes. Every single energy point is calculated by performing geometry optimization with a constrained electrode-electrode separation. Therefore the equilibrium geometry is obtained as the distance at which the total energy is minimal. Due to the failure of DFT-GGA exchange correlation functionals to account for vdW interactions, we optimize the electrode-electrode separation using vdW density functionals optB88-vdW[26] for junctions with physisorbed contacts. Figures 6(a) and 6(b) show the optimized monolayer junction geometries with equilibrium electrode-electrode distance for *trans* and *cis* configurations, respectively.

We show the PDOS of the azobenzene molecules in the monolayer junctions in Fig. 5. As compared to the PDOS of the bare monolayer on Au(111) surface, it can be clearly seen that all molecular orbital levels, including the HOMO and the

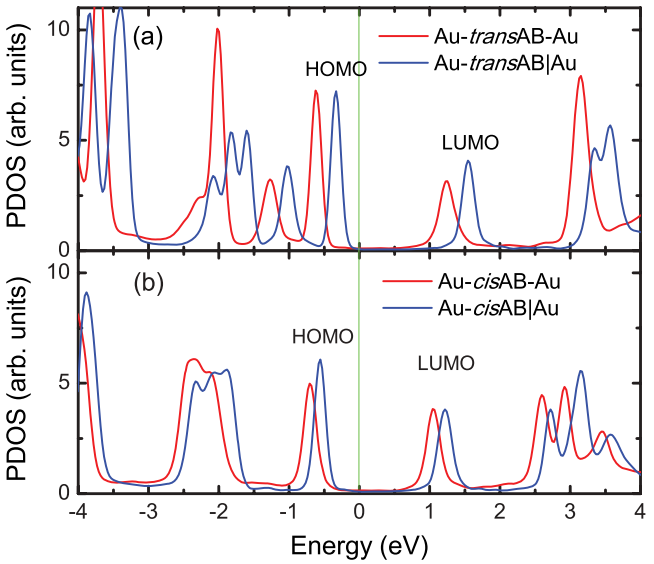


FIG. 5. (Color online) Projected density of states of the molecule in *trans* (a) and *cis* (b) azobenzene monolayer junctions.

LUMO, are shifted to lower energies with the presence of a top monolayer-electrode contact. In Fig. 5(a), the downshift of molecule orbital levels in the Au-*trans* AB|Au junction is only minimal, as compared to Fig. 4(a), primarily because of a weak bonding between the top electrode and the *trans* AB molecule. In contrast, with the sulfur linkers in the top contact of the Au-*trans* AB-Au junction, a stronger monolayer-electrode bonding significantly lowers all molecular orbital levels in energies by about 0.3 eV. The downshift is even more significant in *cis* configurations as shown in Fig. 5(b). All *cis* azobenzene orbital levels shift to lower energies by about 0.4 eV in Au-*cis* AB|Au and 0.6 eV in Au-*cis* AB-Au, compared to Fig. 4(b).

### B. Transmission functions at zero bias

In Figs. 6(c) and 6(d) we show the calculated transmission functions at zero bias for azobenzene monolayer junctions with *trans* and *cis* configurations, respectively. For the Au-*trans* AB-Au junction with chemisorbed top contact, the transmission function has three broad resonance peaks with nearly perfect transmission amplitudes shown in the given range of energy from −2 to 2 eV related to the Fermi energy of the Au electrodes: two are below the Fermi energy (about −1.6 and −0.7 eV), and the third is above it (about 1.1 eV). These three transmission peaks can be directly associated with the frontier molecular orbitals HOMO-1, HOMO, and LUMO, respectively, despite some minor changes in the energy as compared to the PDOS in Fig. 5 due to the periodic boundary condition used in the supercell calculation for PDOS. The transmission peak associated with the HOMO of *trans* azobenzene is relatively narrower in width and lower in height because the HOMO is more localized in the N pair of the molecule and thus contributes less to the electron transmission. These resonance peaks in the transmission function are away from the Au Fermi level, and zero-bias conductance of the monolayer junction is primarily dominated by nonresonance electron tunneling at the Fermi level, with a

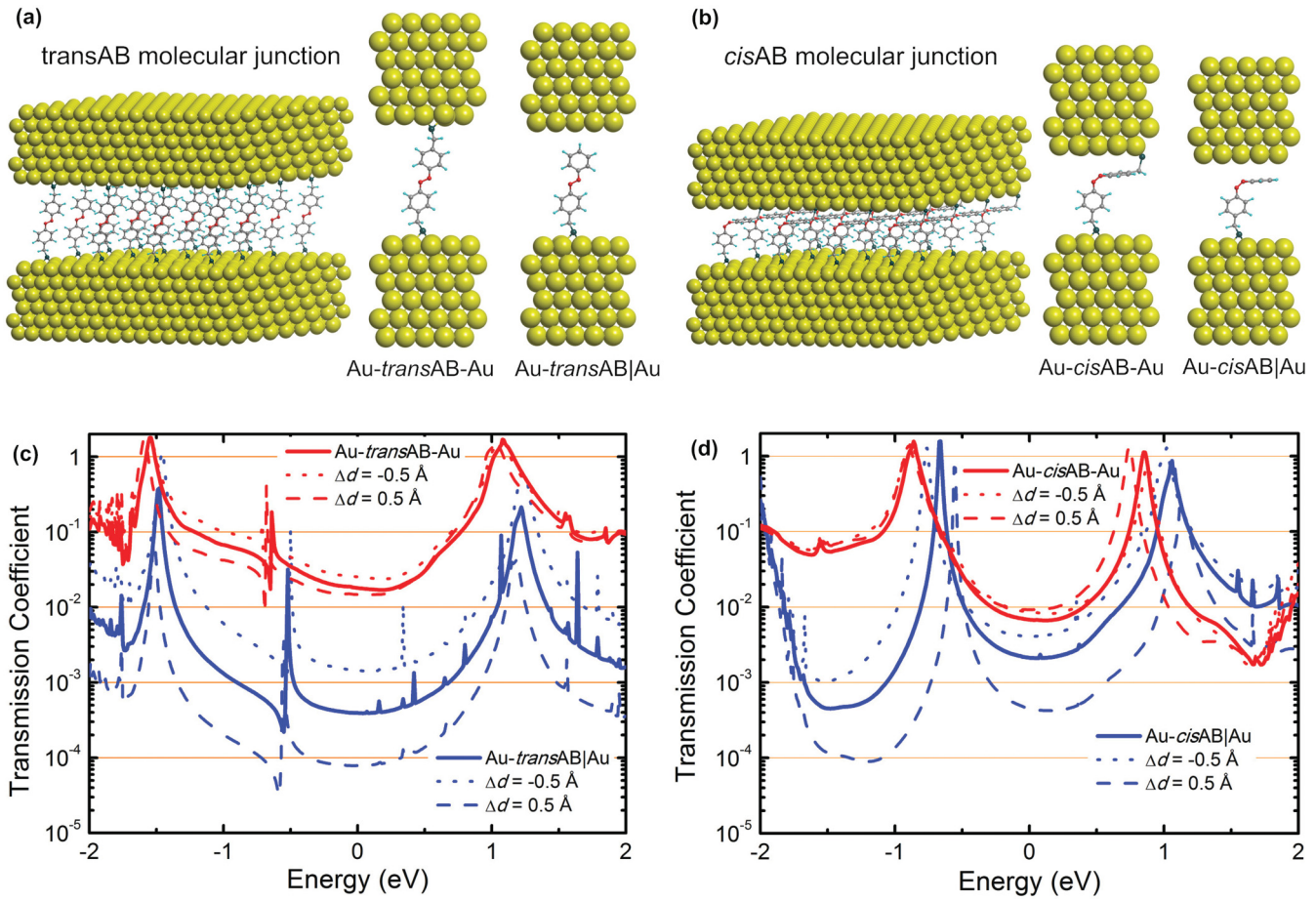


FIG. 6. (Color online) Equilibrium geometries (a), (b) and zero-bias electron transmission functions (c), (d) of *trans* and *cis* monolayer junctions with two types of top contact. In panels (c) and (d) the $y$ axis is in logarithm scale, and the Fermi level is shifted to 0. $\Delta d$ represents the change in the electrode-electrode separation for a junction with its geometry slightly away from the equilibrium structure.

transmission coefficient $T \approx 0.02$. For the Au-*trans* AB|Au junction with a physisorbed top contact, we find that the calculated transmission function is significantly decreased by about two orders of magnitudes compared to that of the Au-*trans* AB-Au junction, and, at the Fermi level, $T \approx 0.0004$. The resonance transmission peaks of the Au-*trans* AB|Au junction shift about 0.2 eV upward in the energy, which follows closely the peaks in PDOS as shown in Fig. 4(a). Besides three major peaks, there are several small resonance peaks appearing in the transmission function of Au-*trans* AB|Au around 0 to 1.2 eV which are induced by the vacuum gap in the top contact. Their relatively smaller amplitudes provide only finite contributions to the tunneling current under certain bias voltages, which we will discuss later in the next section.

For monolayer junctions with the *cis* configuration, however, removing the $CH_2S$ linkers in the top contact leads to a relatively much smaller decrease in transmission function near the Fermi energy, as shown in Fig. 6(d). The transmission functions at the Fermi level for junctions Au-*cis* AB-Au and Au-*cis* AB|Au are $T \approx 0.006$ and 0.002, respectively. For both Au-*cis* AB-Au and Au-*cis* AB|Au, within the given range of energy, two resonance peaks can be found in the transmission functions, which are associated with the *cis* azobenzene HOMO and LUMO. They are also away from the Au Fermi level, and the peaks of Au-*cis* AB-Au junction are lower in energy than that of Au-*cis* AB|Au, corresponding to the PDOS peaks as shown in Fig. 4(b).

The above calculated zero-bias transmission function cannot be simply studied by its relation to the electrode-electrode separation or the azobenzene molecular length. Instead, we can describe the total transmission function that reflects the efficiency of electronic transport from one electrode to the other through the azobenzene monolayer junction as

$$T = T_{\mathrm{bc}}\, T_{\mathrm{mol}}^{\mathrm{p1}}\, T_{\mathrm{mol}}^{\mathrm{p2}}\, T_{\mathrm{tc}}, \tag{3}$$

where $T_{\mathrm{bc}}$ and $T_{\mathrm{tc}}$ give the efficiency of electron transport across the bottom and top contacts, and $T_{\mathrm{mol}}^{\mathrm{p1}}$ and $T_{\mathrm{mol}}^{\mathrm{p2}}$ reflect the electron transport through the first (bottom half) and second (top half) parts of the azobenzene molecule, respectively. From Figs. 6(a) and 6(b), it is safe to assume that the first term $T_{\mathrm{bc}}$ in the above transmission equation is the same for all four junctions. However, the other three terms, $T_{\mathrm{mol}}^{\mathrm{p1}}$, $T_{\mathrm{mol}}^{\mathrm{p2}}$, and $T_{\mathrm{tc}}$, are quite different from case to case, resulting in different total transmission coefficients at the Fermi energy for the above junctions. In the case of the symmetric Au-*trans* AB-Au junction, we have $T_{\mathrm{mol}}^{\mathrm{p1}} = T_{\mathrm{mol}}^{\mathrm{p2}}$ and $T_{\mathrm{bc}} = T_{\mathrm{tc}}$, and the junction has a large transmission coefficient at the Fermi level,

$T \approx 0.02$. The absence of the $CH_2S$ linker in the Au-*trans* AB|Au junction causes a large decrease in $T_{tc}$, and reduces the total transmission coefficient to $T \approx 0.0004$. One may expect such a large change in the transmission term $T_{tc}$ to also apply to the *cis* configuration junction. However, as shown in Fig. 6(d), the total transmission coefficient for Au-*cis* AB|Au ($T \approx 0.002$) is only about three times smaller than that for Au-*cis* AB-Au ($T \approx 0.006$). This clearly indicates that, in the Au-*cis* AB|Au junction, the transmitted electrons travel directly from the bottom contact to the top contact through only the first (bottom) part of the *cis* azobenzene molecule, and avoid the second (top) part of the molecule. Thus for the Au-*cis* AB|Au junction the effective tunneling pathway is greatly reduced, resulting in a total transmission function $T = T_{bc}\, T_{mol}^{p1}\, T_{tc}$. Note this is equal to Eq. (3) with term $T_{mol}^{p2} = 1$ that compensates for the smaller term $T_{tc}$ of the Au-*cis* AB|Au junction, resulting in a smaller difference in the total transmission coefficients between the Au-*cis* AB|Au and Au-*cis* AB-Au junctions as compared to that of the junctions in the *trans* configuration.

It should be also noted that the transmission terms $T_{mol}^{p1}$ and $T_{mol}^{p2}$ are also different between junctions with *trans* and *cis* configurations. Nonresonant electron transmission through a molecule $T_{mol}$ can be empirically expressed as $T_{mol} = \exp(-\beta l)$, where $l$ is the length of the molecule and represents the width of the effective tunneling barrier, and $\beta$ is the tunneling decay factor given by $\beta = (2\sqrt{2m^*\phi}\alpha)/\hbar$ where $\phi$ is the barrier height for tunneling that is determined by the frontier molecular orbital level related to the Fermi energy, $\phi = E_F - E_{MO}$, $m^*$ is the effective mass and $\alpha$ is the shape constant of the barrier. For junctions with chemisorbed top contact, at the Fermi energy the total transmission ratio between *trans* and *cis* configurations is $t = T_{mol}^{trans}/T_{mol}^{cis} = \exp[(\beta_{cis} - \beta_{trans})2l]$. Giving $t \approx 3.3$ from Fig. 6 and $l \approx 4.5$ Å estimated from the length of each half of the azobenzene molecule (remain unchanged upon switching), we have $\beta_{cis} - \beta_{trans} = 0.13$ Å$^{-1}$. For junctions with physisorbed top contact, from the above discussions we know that in the Au-*trans* AB|Au the effective barrier width for the expression of $T_{mol}^{trans}$ is $2l$ and that in Au-*cis* AB|Au is $l$, thus the total transmission ratio between these two junctions at the Fermi energy should be $t' = \exp[(\beta_{cis}l - \beta_{trans}2l)]$. Giving $t' \approx 0.2$ from Fig. 6, we get the tunneling decay factors $\beta_{trans} = 0.49$ Å$^{-1}$ and $\beta_{cis} = 0.62$ Å$^{-1}$. Both of them are in good agreement with the literature values ($\beta \approx 0.4$–$0.6$ Å$^{-1}$) commonly obtained for short $\pi$-conjugated molecules.[27] A possible cause for a smaller tunneling decay factor $\beta_{trans}$ than $\beta_{cis}$ could be the fact that the HOMO levels of the junction in the *trans* configuration lie closer to the Fermi level than the HOMO levels of the junction in the *cis* configuration, as shown in Figs. 5 and 6, resulting in a lower tunneling barrier, $\phi$. The barrier shape constant $\alpha$ could also be affected after the switching of azobenzene monolayer from *trans* to *cis* form.

In experiments, the monolayer-electrode contact of the junction may not be exactly at its equilibrium position, but rather may be slightly stretched or compressed. To simulate this situation, we calculated the transport properties of junctions with an increased (or decreased) electrode-electrode separation $\Delta d = 0.5$ Å(or $\Delta d = -0.5$ Å) with regard to its equilibrium value ($\Delta d = 0$) for both *trans* and *cis* monolayer junctions. The transmission results for stretched and compressed junctions are also shown in Fig. 6. We find that the conductance of the Au-AB-Au junction with chemisorbed top contact is insensitive to the change of $\Delta d$ for both *trans* and *cis* configurations, where as for Au-AB|Au junctions with physisorbed top contact, a small change in the electrode-electrode separation in either direction changes the conductance significantly. This demonstrates that with a physisorbed top contact, the total transmission function of the monolayer junction is highly related to the $T_{tc}$ (contribution from the contact) which is very sensitive to the monolayer-electrode contact distance. In the case of Au-*cis* AB|Au junctions, we also notice that the two peaks in the transmission function at about $-0.7$ and 1.1 eV, which are associated with the HOMO and the LUMO, move up in energy with increased electrode-electrode separation. This phenomenon has also been noticed for other stretched molecular junctions,[28] in which the shift of HOMO resonance in the transmission function toward the Fermi level increases the transmission coefficient at the Fermi energy. However, here the decrease in the transmission coefficient at the Fermi level, due to the stretching of the junction, is much more significant. The transmission peak associated with the *cis* HOMO is still more than 0.5 eV away from the Fermi level with $\Delta d = 0.5$ Å, making the decrease in low bias conductance unlikely to be compensated. In contrast, for stretched and compressed Au-*trans* AB|Au junctions we do not see such obvious changes in the positions of transmission resonances.

To understand the possible influences of the monolayer tilt angle $\theta$ on the transport properties, we carried out further calculations for Au-*trans* AB-Au junction with different $\theta$. The optimized junction structures with 45° or 10° tilted *trans* monolayer are shown in Figs. 7(a) and 7(b), respectively. A large change in the electrode-electrode separation occurs between these two cases ($\Delta_d = 2.5$ Å). However, as shown in Fig. 7(c), for junctions with a 45° or 10° tilted *trans* monolayer, we find essentially the same features in the transmission functions as those obtained for the optimized geometry with $\theta = 20°$, yet with a small change in position of transmission resonance peaks associated with the *trans* azobenzene molecular orbital levels for $\theta = 45°$. The transmission at the Fermi level for 45° tilted junction is only slightly increased as compared to the junctions with small tilt angles. The source of this increase is the downward shifting of the broad peak in the transmission function associated with the *trans* LUMO. The shifting of molecular frontier levels resulting from the change in tilt angle may result from a change in the effective dipole moment as well as the work function at the molecule-metal interfaces.[29] Similar phenomena have also been noticed in tilted alkanethiol monolayers,[30] in which the tilt brings the HOMO resonance closer to the Fermi energy. Nevertheless, we conclude that for dilute monolayer junctions without intermolecular contribution, the molecular tilt has very little effect on its conductance since the effective tunneling pathway through the molecule remains unchanged upon tilting.

### C. Current-voltage characteristics

The self-consistently calculated current-voltage characteristics (*I*-*V*) of Au-AB-Au and Au-AB|Au junctions are

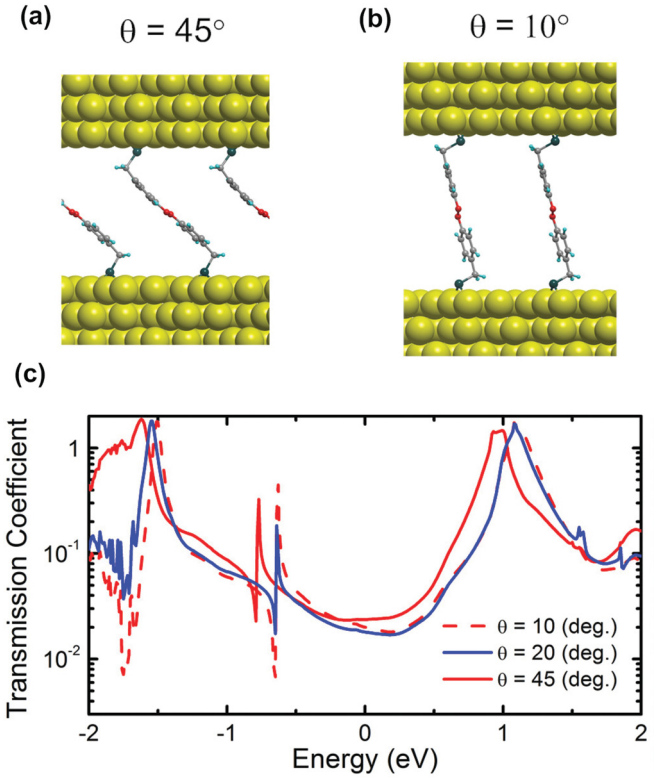


FIG. 7. (Color online) Equilibrium geometries and zero-bias transmission functions for Au-*trans* AB-Au junctions with a tilt angle $\theta$ of 45° and 10°.

depicted in Figs. 8(a) and 8(b), respectively. For the Au-*trans* AB-Au junction, a highly symmetric *I*-*V* curve arises as expected with two symmetric monolayer-electrode contacts, and its current is larger than that of the Au-*cis* AB-Au junction

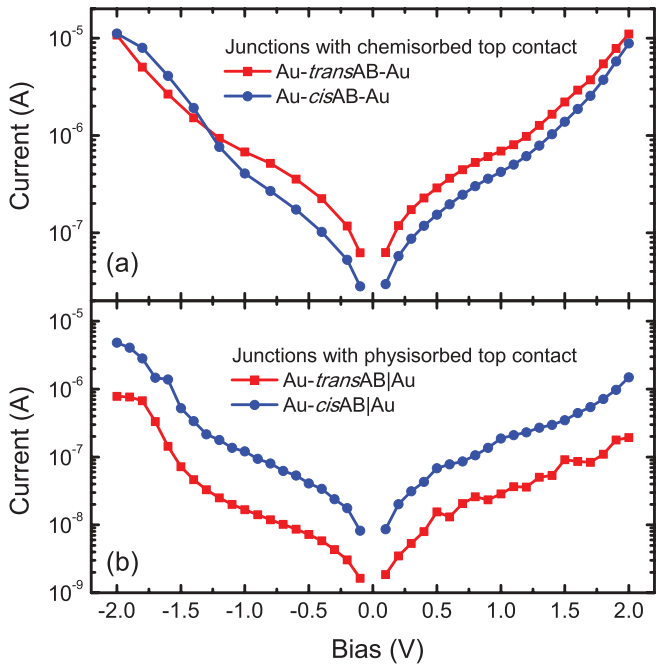


FIG. 8. (Color online) Current voltage characteristics of Au-AB-Au and Au-AB|Au junctions with *trans* and *cis* configurations.

in small bias region, consistent with the zero-bias transmission functions. Thus, with chemisorbed top contact, the two isomers realize different conductance states of the monolayer junction corresponding to ON (*trans* configuration) and OFF (*cis* configuration). The current of the Au-*trans* AB-Au junction becomes smaller than that of the Au-*cis* AB-Au only in the region of large negative bias voltage (−1.2 to −2.0 V). This can be attributed to the fact that the Au-*cis* AB-Au junction is asymmetric in geometry, resulting in an asymmetric *I*-*V* curve which has a slightly larger current in the large negative bias region. Such asymmetric behavior is also shown in the *I*-*V* curves for junctions Au-*trans* AB|Au and Au-*cis* AB|Au, with asymmetric top (physisorbed) and bottom (chemisorbed) contacts. Nonetheless, for junctions with a physisorbed top contact, the *cis* configuration (ON state) exhibits a larger current for any given voltage than that of the *trans* configuration (OFF state), and the ON/OFF ratio of the current is more pronounced than that of the junctions with chemisorbed top contacts. These theoretical results for junctions with a physisorbed top contact are, therefore, in reasonable qualitative consistency with the reported measurements.[8–10] A quantitative matching of the ON/OFF ratio to the experiments is not expected because the length of the molecules in experiments are much longer than those in our study.

In Fig. 8(b), we find the current of the Au-*trans* AB|Au junction oscillates as a function of positive bias voltage, which corresponds to the small resonance peaks found in the transmission function above the Fermi level as shown in Fig. 6(c). As we increase the voltage, these resonance peaks sequentially join the bias window and contribute to the current, resulting in a resonant tunneling current at certain bias voltages. However, these resonances can only provide finite contributions to the current in the *trans* configuration, and the current ratio between the *trans* and *cis* configurations is almost unaffected.

### D. Effect of molecular packing density

The above calculations are based on a diluted monolayer structure with a low packing density, in which the intermolecular bonding between molecules in the monolayer can be considered negligible and junction transport properties are primarily dominated by the intramolecular contribution. To inquire into the effect of intermolecular interaction on the transport, Au-AB-Au junctions with a higher monolayer packing density are also considered, in which the molecules are positioned closer to each other to increase the molecular interactions. In this case for each junction we have two azobenzene molecules per $(\sqrt{3} \times \sqrt{3})R30°$ Au(111) unit cell, and the packing area corresponds to 45.4 Å per molecule. The optimized junction structures for *trans* and *cis* configurations are shown in Figs. 9(a) and 9(b), and we denote them as Au-2*trans* AB-Au and Au-2*cis* AB-Au, respectively. For the *cis* configuration, as compared to the Au-*cis* AB-Au junction with a low packing density, we see that the azobenzene molecules in the monolayer of the Au-2*cis* AB-Au junction become distorted, so that the top half of the molecule is no longer parallel to the top Au surface but instead rotated relative to the Au surface, resulting from an increased intermolecular interaction with decreased spacing between the molecules.

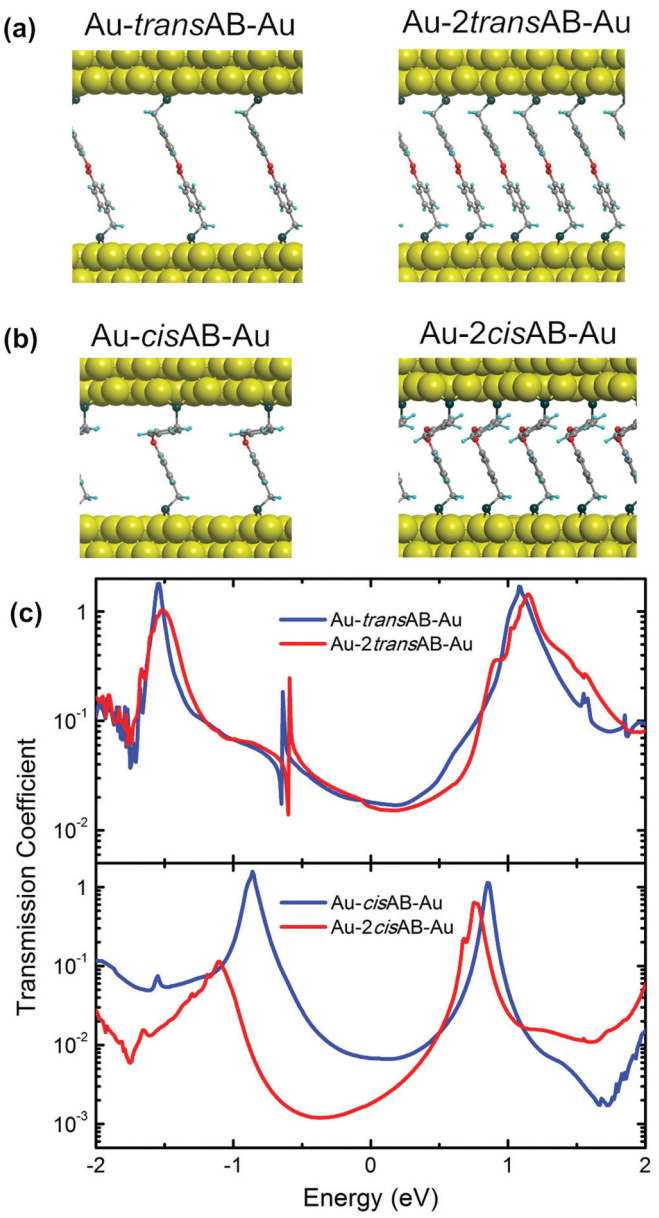


FIG. 9. (Color online) Equilibrium geometries and zero-bias transmission functions of azobenzene monolayer junctions with different packing density. The calculated transmission coefficients for junctions with high monolayer packing density are divided by two (number of azobenzene molecules in one cell) in order to compare with the results with low packing density.

The calculated zero-bias transmission functions are shown in Fig. 9(c). For the *trans* configuration, doubling the packing density produces only negligible changes in transmission function. However, for the *cis* configuration, the junction's transmission coefficients are significantly reduced especially in the energy region around the Fermi level. The decrease in conductance by increasing the packing density has also been observed in other monolayer junctions,[13] but the reason has been attributed to a shift of the LUMO resonance peak in the transmission function to a higher energy away from the Fermi level. Our result differs from that in Ref. 13 in that the LUMO peak in the transmission function of the Au-2*cis* AB-Au junction slightly shifts to a lower energy which is closer to the Fermi level as compared to the Au-*cis* AB-Au. Nevertheless, the transmission coefficients for the HOMO resonance peak and for the energy region around the Fermi level are decreased by about one order of magnitude. The considerable decrease in the transmission function can be attributed to the geometry distortion in the *cis* azobenzene monolayer which is caused by intermolecular interactions with the dense packing, as shown in Fig. 9(b). Our results show clearly that interaction among the azobenzene molecules of the monolayer junction can induce large changes in transport in the *cis* configuration, hence suggesting that a higher conductance ON/OFF ratio can be achieved in densely packed azobenzene monolayer junctions with chemisorbed monolayer-electrode contact. For junctions with a physisorbed contact, since the ON state is associated with the *cis* configuration, we expect that increasing the monolayer packing density could decrease the conductance ON/OFF ratio.

### E. Effect of top-contact geometry

Having addressed the transport properties of azobenzene molecular junctions with a perfect contact surface at the monolayer-electrode interface, it is necessary to also study the consequences of nonideal situations. To investigate the role of contact atomic structure, we consider a simple but possible situation: the sulfur atom bound to a single Au atom protruding from the surface of the top Au electrode, which is shown in Figs. 10(a) and 10(b) for *trans* and *cis* configurations, and we denote them as Au-AB-$Au_1$-Au and Au-2*cis* AB-Au, respectively. The purpose of this consideration is to simulate possible situations in experiments in which the surface of the top electrode may not be atomically flat when contacting the molecules in the monolayer.

The calculated transmission functions are shown in Fig. 10(c). We find that the additional Au atom decreases the transmission coefficients at nonresonance tunneling regions in the transmission function for both *trans* and *cis* configurations, as compared to Fig. 6. Moreover, the resonance peaks in the transmission functions associated with the frontier molecular orbitals all shift up in energy at a noticeable change. The HOMO transmission resonance of Au-*trans* AB-$Au_1$-Au junction shifts from $-0.7$ to $-0.4$ eV; while that of Au-*cis* AB-Au junction shifts from $-0.85$ to $-0.2$ eV, which is very close to the Fermi energy.

In Fig. 10(d) we show the calculated current-voltage characteristics for Au-AB-$Au_1$-Au junctions. The most noticeable feature appearing in Fig. 10(d) is the asymmetry in the *cis* configuration. For a negative bias voltage below 1 eV, the current through the *cis* configuration is significantly higher than the current through the *trans* configuration. As the negative bias is further increased, the current through the *cis* configuration decreases dramatically with increasing voltage, resulting in a region of negative differential resistance (NDR). This NDR feature also appears in the positive bias region (from 1.2 to 1.7 V) in the *cis* configuration, but is not present for any bias region in the *trans* configuration. In contrast to Au-*cis* AB-$Au_1$-Au, the *I*-*V* characteristics of Au-*trans* AB-$Au_1$-Au junction are basically unchanged by the presence of the additional Au atom as compared to Fig. 8(a).

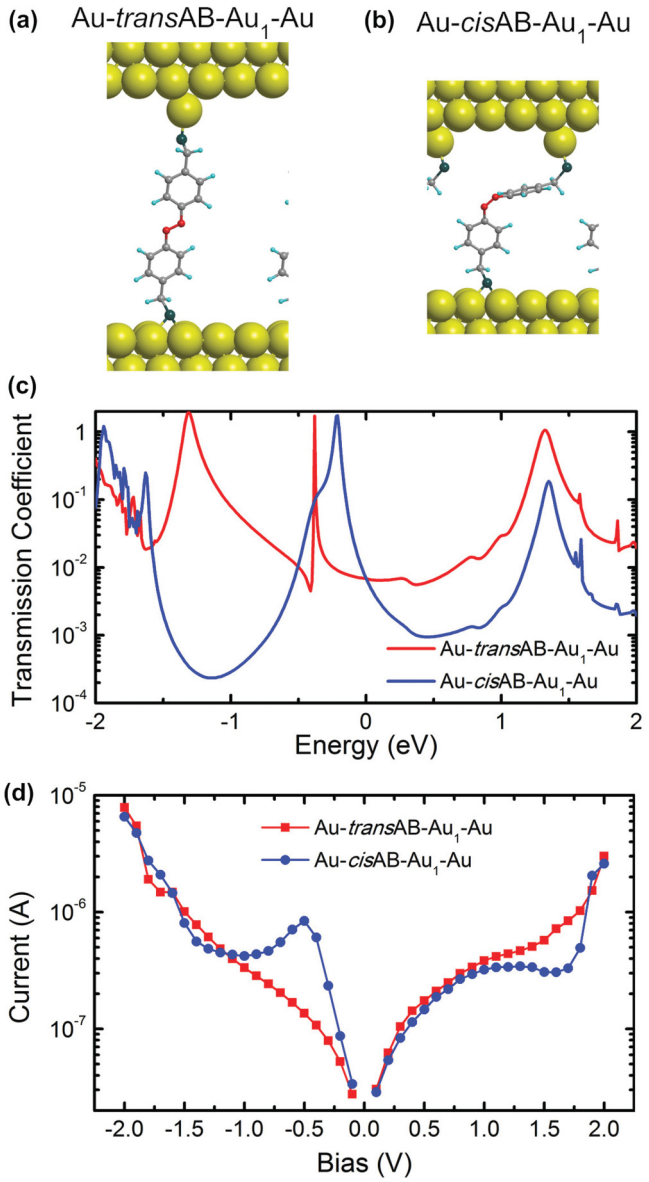


FIG. 10. (Color online) Equilibrium geometries, zero-bias electron transmission coefficients, and current-voltage characteristics of Au-AB-Au$_1$-Au junctions.

To shed light on the origin of the NDR effect, we give the transmission function $T(E,V)$ at a series of biases from $-2.0$ to 2.0 V at 0.5 V intervals as shown in Fig. 11. In the case of the *cis* configuration, a voltage of $-0.5$ V creates a bias-induced transmission peak at about $-0.2$ eV (marked with an arrow in Fig. 11) adjacent to the resonance peak associated with molecular LUMO. As the negative bias is further increased, this transmission peak, with a broad width, moves up in energy and toward the molecular LUMO resonance. It dominates the transmission function within the bias window, thus raising a much larger current than that at positive bias and resulting in a noticeable rectification effect for Au-*cis* AB-Au$_1$-Au junction in Fig. 10(c). In the case of *trans* configuration, however, only several bias-induced transmission peaks exist at positive bias, and all of them have much lower amplitudes and shorter widths leading to only small current contributions. Correspondingly,

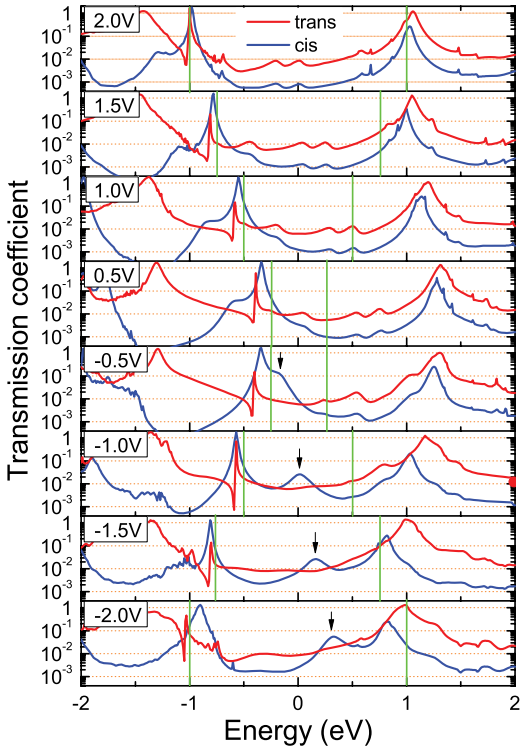


FIG. 11. (Color online) Electron transmission coefficients of Au-AB-Au$_1$-Au junctions with *trans* and *cis* configurations under various bias voltages from $-2.0$ to 2.0 V. The region between two green vertical lines indicates the bias window. Arrows indicate the bias-induced transmission peaks in the transmission functions in the *cis* configuration.

in Fig. 10(c) the rectification behavior in the *I*-*V* curve of Au-*trans* AB-Au$_1$-Au junction is not obvious and there is no NDR effect. This demonstrates that the azobenzene monolayer junction can be used for a photocontrolled molecular rectifier with proper engineering of its contact geometry.

It should also be noted that for both *trans* and *cis* configurations, the bias drives the LUMO resonance peak away from the Fermi level, so its contribution to the current becomes important only at a sufficiently large bias (e.g., $V \approx 2$ V) which should be comparable to the HOMO-LUMO gap of the molecule. This is also true for the calculated *I*-*V* characteristics in Sec. IV C. Therefore, at low bias the electronic transport of all the monolayer junctions in consideration is mainly facilitated by nonresonant electron tunneling.

## V. CONCLUSION

Our first-principles calculations indicate that monolayer-electrode bonding, intermolecular interaction, and contact geometry all play very important roles in determining the conductance ratio of azobenzene monolayer junction between *trans* and *cis* configurations. With a strongly bonded top contact from chemisorption, the zero-bias transmission of *trans* monolayer is higher than that of the *cis* monolayer. Replacing it by a weakly bonded contact with physisorption will decrease the conductance by about two orders of magnitudes for the *trans* monolayer. However, in the case of the *cis* configuration, the

physisorbed contact shortens the effective tunneling pathway, leading to a conductance that is less sensitive to weak bonding. The mechanisms are interpreted by applying a simple transmission model to the calculated zero-bias transmission functions, which accounts for electron transmission through each subunit of the molecular junction and provides a clear physical picture for understanding the junction. The calculated current-voltage characteristics indicate that for junctions with physisorbed top contact, the ON state with larger current is associated with the *cis* configuration, which is in agreement with recent experiments. Our calculations demonstrate that the intermolecular interaction in the *trans* configuration is negligible even in a densely packed monolayer; while for the *cis* configuration, increasing the monolayer density causes a considerable distortion in the monolayer structure, resulting in a decrease in its transmission function thus increasing the conductance ratio. We also find that the calculated current-voltage characteristics for the *trans* monolayer remain symmetric upon changing of the top contact geometry. In contrast, a slightly modified contact geometry will affect the electric current through the *cis* monolayer, leading to a highly unsymmetrical current-voltage curve as well as a large negative differential resistance behavior. These results suggest that the molecule-lead contact, the state of the molecule, the morphology of the metal surface, and the packing density of the monolayer are all parameters in the play. Our investigations thus will deepen understanding of electron transport through azobenzene monolayer junctions.

## ACKNOWLEDGMENTS

This work is supported by US/DOE/BES/DE-FG02-02ER45995. The authors acknowledge DOE/NERSC and UF-HPC centers for providing computational resources.

[1] M.-M. Russew and S. Hecht, Adv. Mater. **22**, 3348 (2010).
[2] S. J. Molen and P. Liljeroth, J. Phys. Condens. Matter **22**, 133001 (2010).
[3] C.-W. Chang, Y.-C. Lu, T.-T. Wang, and E. W.-G. Diau, J. Am. Chem. Soc. **126**, 10109 (2004).
[4] T. Ikegami, N. Kurita, H. Sekino, and Y. Ishikawa, J. Phys. Chem. A **107**, 4555 (2003).
[5] C. Zhang, M.-H. Du, H.-P. Cheng, X.-G. Zhang, A. E. Roitberg, and J. L. Krause, Phys. Rev. Lett. **92**, 158301 (2004).
[6] C. Zhang, Y. He, H.-P. Cheng, Y. Xue, M. A. Ratner, X.-G. Zhang, and P. Krstic, Phys. Rev. B **73**, 125445 (2006).
[7] M. Valle, R. Gutiérrez, C. Tejedor, and G. Cuniberti, Nat. Nanotechnol. **2**, 176 (2007).
[8] V. Ferri, M. Elbing, G. Pace, M. D. Dickey, M. Zharnikov, P. Samori, M. Mayor, and M. A. Rampi, Angew. Chem. Int. Ed. **47**, 3407 (2008).
[9] J. M. Mativetsky, G. Pace, M. Elbing, M. A. Rampi, M. Mayor, and P. Samori, J. Am. Chem. Soc. **130**, 9192 (2008).
[10] K. Smaali, S. Lenfant, S. Karpe, M. Oçfrain, Philippe Blanchard, D. Deresmes, S. Godey, A. Rochefort, J. Roncali, and D. Vuillaume, ACS Nano **4**, 2411 (2010).
[11] X. D. Cui, A. Primak, X. Zarate, J. Tomfohr, O. F. Sankey, A. L. Moore, T. A. Moore, D. Gust, G. Harris, and S. M. Lindsay, Science **294**, 571 (2001).
[12] J. Taylor, M. Brandbyge, and K. Stokbro, Phys. Rev. Lett. **89**, 138301 (2002).
[13] L. A. Agapito, C. Cao, and H.-P. Cheng, Phys. Rev. B **78**, 155421 (2008).
[14] G. Kresse and J. Furthmüller, Comput. Mater. Sci. **6**, 15 (1996).
[15] M. Brandbyge, J. L. Mozos, P. Ordejón, J. Taylor, and K. Stokbro, Phys. Rev. B **65**, 165401 (2002).
[16] S. Datta, *Electronic Transport in Mesoscopic Systems* (Cambridge University Press, Cambridge, England, 1995).
[17] J. M. Soler, E. Artacho, J. D. Gale, A. García, J. Junquera, Pablo Ordejón and D. Sánchez-Portal, J. Phys. Condens. Matter **14**, 2745 (2002).
[18] J. P. Perdew, K. Burke, and M. Ernzerhof, Phys. Rev. Lett. **77**, 3865 (1996).
[19] H. J. Monkhorst and J. D. Pack, Phys. Rev. B **13**, 5188 (1976).
[20] K. Momma and F. Izumi, J. Appl. Crystallogr. **44**, 1272 (2011).
[21] E. McNellis, J. Meyer, A. D. Baghi, and K. Reuter, Phys. Rev. B **80**, 035414 (2009).
[22] F. W. Schulze, H. J. Petrick, H. K. Cammenga, and H. Klinge, Z. Phys. Chem. Neue Folge **107**, 1 (1977).
[23] G. Henkelman, A. Arnaldsson, and H. Jónsson, Comput. Mater. Sci. **36**, 254 (2006).
[24] S. Alkis, P. Jiang, L.-L. Wang, A. E. Roitberg, H.-P. Cheng, and J. L. Krause, J. Phys. Chem. C **111**, 14743 (2007).
[25] C. Chapman and I. Paci, J. Phys. Chem. C **114**, 20556 (2010).
[26] J. Klimeš, D. R. Bowler, and A. Michaelides, Phys. Rev. B **83**, 195131 (2011).
[27] A. Salomon, D. Cahen, S. Lindsay, J. Tomfohr, V. B. Engelkes, and C. D. Frisbie, Adv. Mater. **15**, 1881 (2003).
[28] Y. Xue and M. A. Ratner, Phys. Rev. B **68**, 115407 (2003).
[29] V. De Renzi, R. Rousseau, D. Marchetto, R. Biagi, S. Scandolo, and U. del Pennino, Phys. Rev. Lett. **95**, 046804 (2005).
[30] T. Frederiksen, C. Munuera, C. Ocal, M. Brandbyge, M. Paulsson, D. Sanchez-Portal, and A. Arnau, ACS Nano **3**, 2073 (2009).